MITEx: a portable hand exoskeleton for assessment and treatment in neurological rehabilitation

Davide Astarita[1,2], Jun Pan*[1,2], Lorenzo Amato[1,2], Paolo Ferrara*[1,2], Andrea Baldoni[1,2], Filippo Dell'Agnello[1,2], Simona Crea[1,2,3], Nicola Vitiello[1,2,3] *Member, IEEE,* Emilio Trigili[1,2], *Member, IEEE*

***Abstract*— This work describes the design and preliminary characterization of a novel portable hand exoskeleton for post-stroke rehabilitation. The platform actively mobilizes the index-metacarpophalangeal (I-MCP) joint, and it additionally offers individual rigid support to distal degrees of freedom (DoFs) of the index and thumb. The test-bench characterization proves the capability of the device to render torques at the I-MCP level with high fidelity within frequencies of interest for the application (up to 3 Hz). The introduction of a feed-forward friction compensation at the actuator level lowers the output mechanical stiffness by 32%, contributing to a highly transparent behavior; moreover, the functionality of the platform in rendering different interaction strategies (patient/robot-in-charge) is tested with three healthy subjects, showing the potential of the device to provide assistance *as needed*.**

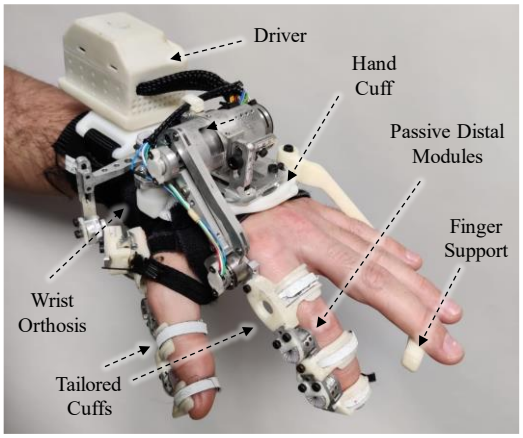

Figure 1 – Overview of the MITEx exoskeleton.

I. Introduction

Upper-limb impairments following a stroke event affect the quality of life of people, especially in case of hand impairments limiting common grasping capabilities. Timed, intense, and tailored robot-aided rehabilitation can be beneficial for an effective recovery of functional movement capabilities and for restoring activities of daily living; nevertheless, only a very limited number of robotic hand exoskeletons leave the laboratory environment and are effectively deployed in clinical facilities [1].

Hand exoskeletons based on soft textiles exhibit characteristics of low weight and ease of setup and are suitable for the rehabilitation of individuals with mild to low impairments, because of the limited torque output [2]. Rigid exoskeletons constitute promising solutions for patients with more severe movement limitations since they can deliver higher assistive torques, by relying on complex kinematic structures (e.g., remote centers of rotations, passive DoFs). Nevertheless, the increased mechanical complexity and encumbrance on the hand forces a careful selection of the number of assisted joints, to maintain a streamlined mechanical design that retains the capability of delivering high power safely and efficiently [3]. In this perspective, addressing the metacarpophalangeal (MCP) joint movement should be prioritized since this joint has been identified as accountable for most of the information in hand control during grasp tasks [4], and finger dexterity can be correlated with the level of functional recovery after stroke [5]. By focusing only on the index finger, it becomes possible to limit the device's weight in favor of compactness and ease of use, maintaining the capability to achieve fine movements (e.g. pinching) required for functional activities.

To increase the portability of hand devices, cable-based solutions can enable remote actuation [6], relieving the limb from the weight of the actuation units; however, they can suffer from friction and backlash that undermine their efficiency of torque transmission.

From the control perspective, modulating the power exchange in human-robot interaction is paramount to render different levels of assistive actions according to the residual capabilities of the user [7]; EMG-based control proved to be effective for continuous passive finger movements [8] or to replicate grasping tasks based on user's intention [9], even though it requires subject-specific calibration procedures and it may be difficult to exploit in patients with poor volitional muscle activity. Series-elastic actuators in force-sensing configuration (FSEAs) allow instead for shared cooperative human-robot control via high-fidelity torque control by measuring directly the torque delivered to the user [10]. Finally, *transparency* of the device, intended as its capacity of rejecting disturbance interaction torques [11], becomes a relevant feature for both a comfortable use and its exploitation in clinics also as an assessment tool to measure biomechanical parameters relevant to clinical assessment (e.g, movement

This research was supported by the EU Commission through the H2020 ReHyb project (Rehabilitation based on hybrid neuroprosthesis, Grant Agreement: 871767).

[1]The Biorobotics Institute, Scuola Superiore San'Anna, 56025 Pontedera, Italy.

[2]Department of Excellence in Robotics & AI, Scuola Superiore Sant'Anna, 56127 Pisa, Italy.

[3]IRCCS Fondazione Don Gnocchi, Florence, 50143, Italy. They have commercial interests in IUVO S.r.l., a spinoff company of Scuola Superiore Sant'Anna.

* J.P. and P.F. were with The Biorobotics Institute and with Department of Excellence in Robotics & AI.

Corresponding author: davide.astarita@santannapisa.it

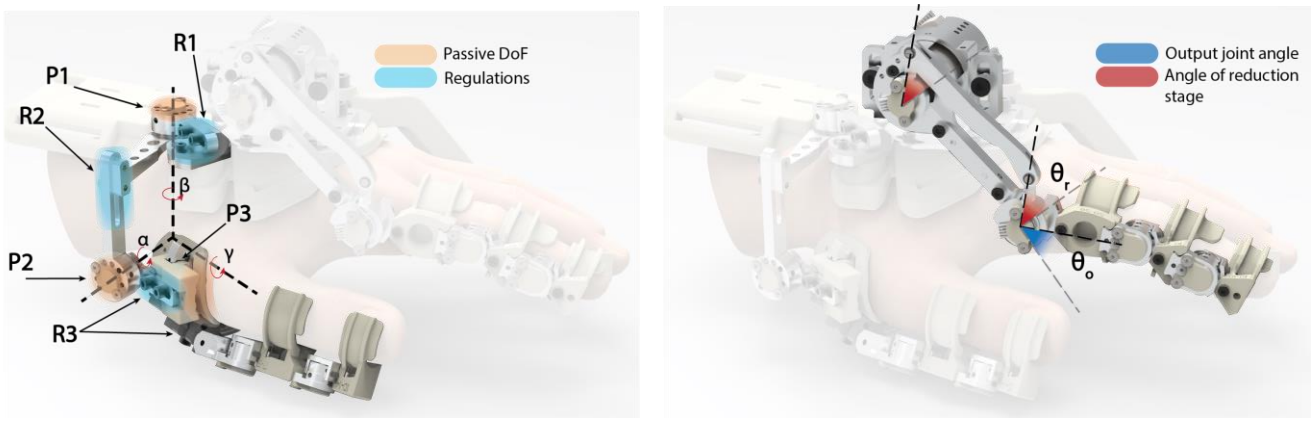

Figure 2 - Kinematic chain for the passive thumb module (left), and for the active transmission system (on the right)

smoothness).

Based on such considerations, this work presents a novel portable exoskeleton for hand neurorehabilitation, namely the Modular Index-Thumb Exoskeleton (MITEx): the device actively assists the index MCP (I-MCP) and it offers rigid support to the other index joints and thumb joints. 3D-printed cuffs available in different sizes allow fitting users with different anthropometries, while a flipping mechanism is embedded to wear the device either on right or left hands. The adopted mechatronics confer transparency at the I-MCP joint, as well as the possibility for customization of the assistance during both single-joint mobilization exercises and pinching and grasping tasks to promote functional recovery in a clinical setting. With this new platform, we strive to investigate and highlight the relevance of MCP joint rehabilitation with a specific focus on the index, in line with recent scientific works [5],[12].

In Section II, a complete description of the platform is provided; Section III presents the results of a preliminary evaluation of the device both on the bench and with the human in the loop; results are discussed in Section IV; finally, Section V draws the conclusions.

II. MITEX EXOSKELETON

A. *Kinematics and interface*

Three main components can be identified in the exoskeleton: the physical Human-Robot Interface (p-HRI), the active index module, and the passive thumb.

A textile commercial wrist orthosis (see Figure 1) ensures comfort and prevents skin irritation or any other nuisance that can potentially arise after prolonged use; a 3D-printed cuff, embedded into the orthosis on the hand dorsum and secured by using Velcro straps, constitutes the support frame for the exoskeleton. Moreover, a mechanical support for the long fingers (apart from the index) is attached to the hand dorsum cuff: accounting for poor finger control in stroke patients, this design sets the palm free not to hinder grasps tasks, and it stabilizes the device with respect to tilting torques by adding a further constraint to the p-HRI.

The **index module** is positioned laterally to the finger, aligning the robotic joint with the human I-MCP. Because of the lack of self-aligning mechanisms, proper manual alignment is paramount for a safe and comfortable operation of the device [13]. For this purpose, tailored 3D-printed C-shaped cuffs for the phalanxes are integrated into the finger kinematic chain. The cuffs are available in different sizes, and their selection is based on the inter-joint distance and phalanx diameter, to mitigate anthropometry discrepancies. They can be quickly replaced and coupled to the phalanx by using Velcro straps. The distal cuff covers only the dorsal side of the phalanx to preserve touch sensory information during pinching tasks, yet guaranteeing rigid force transmission to the fingertip.

The index module is coupled with the proximal interphalangeal (I-PIP) and the distal interphalangeal (I-DIP) articulations by employing two passive modules with a configurable Range of Motion (RoM) in the range [0, 90]°: specifically, two mechanical stops can be set to limit flexion and the extension respectively, and limit the RoM within a specific configuration.

The **thumb module** features a patented design composed of a passive kinematic chain connected to the hand cuff [14]. The chain mimics the movements of the carpometacarpal joint of the thumb (T-CMC), which is modeled as a spherical joint with three intersecting axes (α, β, γ in Figure 2a) enabling the movement and orientation of the metacarpal bone in the 3D-space. These three DoFs, implemented with two revolute joints and a circular guide (P1, P2, and P3 respectively), passively address the movements of thumb ad/abduction, flexion/extension, and opposition, and they can be locked in desired configurations. Manual regulations (R1 and R2) allow the alignment of the virtual center of rotation of the three axes with the anatomical T-CMC. The output of the circular guide P3 is connected to a kinematic chain addressing thumb MCP and interphalangeal joints. The chain is placed laterally with the thumb and includes the same passive, lockable modules employed for the index module. Also in this case, the alignment of the passive modules is eased by the custom 3D-printed cuffs, in addition to one mechanical regulation in the thumb longitudinal direction (R3).

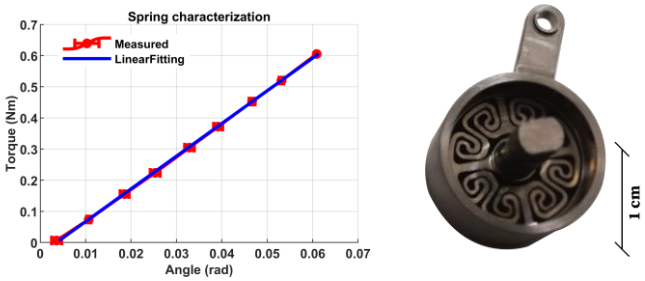

Figure 3 - Characterization data of the spring (on the left), and its design (on the right)

B. *Electronics and Actuation*

A dedicated box embeds the power and control electronics and is responsible for: i) providing power supply through a LiIon battery certified for medical devices, ii) running the firmware, on a custom-designed control board, endowed with a commercial system on module (SbRIO-9651, NI – Austin, Texas, USA), and iii) interfacing the robot with external devices, e.g. a remote PC, via Wifi nano router, improving portability of the platform. The control board features a double PCB layer integrating an FPGA, representing the substrate for sensing, low-level controls and serial interfaces, and a real-time (RT) processor. The electronics box does not hinder upper limb dexterity since it is tethered using a single, compact power and signal cable to the driver (ELMO, Platinum Solo Twitter 15/100). This driver is located above the wrist, close to the motor, firmly fixed on a 3D-printed support, and monitored and controlled via the remote control board using the EtherCAT (ECAT) communication protocol. Even though a small weight (85 g) is added on the limb of the user, the *in-situ* collocation of the motor driver contributes to improving the electrical safety, the portability of the device, and the overall wiring architecture.

The actuation unit is driven by a BLDC motor (2214-BXTH 6W 12V, Faulhaber, Germany) with a reduction stage (rr=108), and it is placed on the hand dorsum cuff. The housing of the actuation unit embeds four regulations to align the actuated joint with the anatomical joint: three of them enable positioning of the actuation unit along the longitudinal, vertical, and mediolateral axis of the hand to comply respectively with different lengths, thicknesses, and widths of the hand; additionally, the last one allows the orientation of the robotic joint around the vertical axis to account for ad/abduction of the I-MCP.

From the output of the actuation unit, a parallelogram transmits the torque to the robotic joint at the I-MCP level by means of a torsional elastic element, realizing an FSEA (Figure 2b). The elastic element is a patented custom spring designed to bear a peak torque of 1.5 Nm [15]; the spring was experimentally characterized on a testbench, showing high linearity of the torque/deformation curve with a stiffness of 10.49 Nm/rad (Figure 3). The spring deflection, from which the torque at the I-MCP (τ) is calculated, is measured by two magnetic encoders (RM08 12 bit, RLS, Slovenija) placed on the output of the actuation unit (angle θ_r), and on the spring output (corresponding also to the measured I-MCP joint angle θ_o), respectively (Figure 2b).

The actuation unit can assist either left or right hands, simply by flipping the parallelogram and changing the interface at the hand dorsum level.

C. *Control*

The control architecture is characterized by three layers arranged hierarchically, namely the high, middle, and low-level control layer (Figure 4); the first, running on the RT processor at 100 Hz, is responsible for generating minimum jerk trajectories for the joint (i.e., a desired angle θ_d). The middle level, also running on the RT processor, is deputed to generating the desired I-MCP interaction torque (τ_d), which can be limited via software to account for safety; τ_d is set based on an impedance control law, based on the error between the desired angle and the measured I-MCP angle θ_o:

$$\tau_d = K_p(\theta_d - \theta_o) + K_d(\dot{\theta}_d - \dot{\theta}_o) \quad (1)$$

The proportional gain K_p, equivalent to a virtual stiffness, can be tuned to render from compliant to stiff behavior, while the derivative contribution offers a stabilizing action.

When the torque reference τ_d is always set to zero, the device operates in the so-called *transparent mode*, rendering the least impedance to the output. Within this modality, the patient is completely in charge of the movement and is capable of freely moving without significant resistance in backdriving the actuation unit.

The low-level control layer, entrusted to the FPGA, implements the closed-loop torque controller, which sets the reference current to the driver; the control loop runs at 500 Hz. As in [16], the torque control input presents 3 different actions: a friction compensation i_f, a feed-forward contribution i_{ff}, and a PD controller:

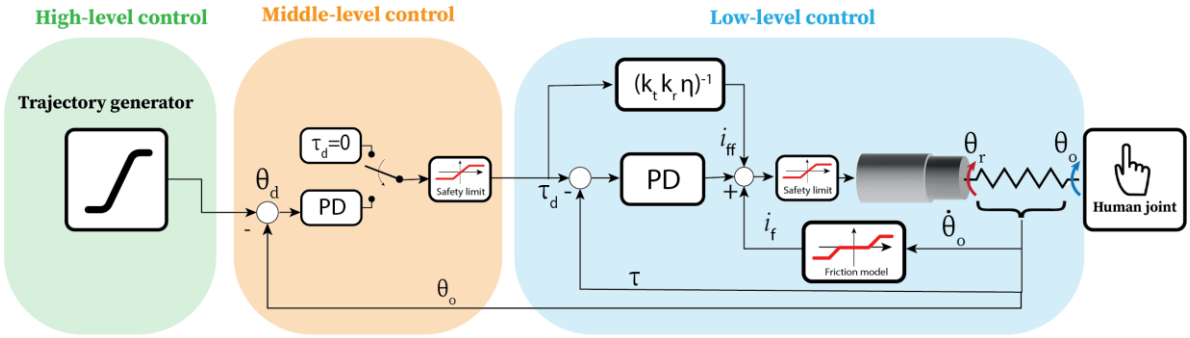

Figure 4 - Layered control architecture

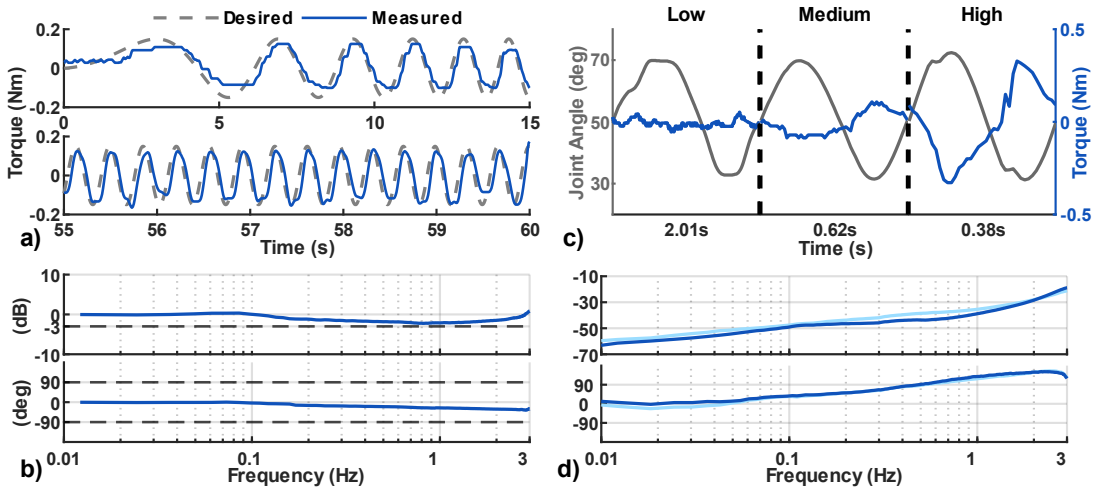

Figure 5 – Test bench characterization: torque tracking a) with respective frequency response b); an example of different frequencies during the transparency test c) and frequency response for residual stiffness d) without (light blue) and with (blue) friction compensation.

$$i_m = i_f + i_{ff} + K_p(\tau_d - \tau) + K_d(\dot{\tau}_d - \dot{\tau}) \qquad (2)$$

The friction compensation term i_f contributes to enhancing transparency according to the following friction model, based on the joint velocity $\dot{\theta}_o$:

$$i_f = \begin{cases} 0 & |\dot{\theta}_o| < \dot{\theta}_{tr} \\ k_f\,(\dot{\theta}_o - \dot{\theta}_{tr} sign(\dot{\theta}_o)) & |\dot{\theta}_o| > \dot{\theta}_{tr} \\ \bar{\imath}_f & i_f > \bar{\imath}_f \end{cases} \qquad (3)$$

The model in (3) adopts a deadband to avoid chattering around the zero-crossing region, limited by $\dot{\theta}_{tr}$, which is equal to twice the maximum noise on the velocity signal measured when the output is not moving. A linear contribution (coefficient $k_f = {\bar{\imath}_f}/{5\dot{\theta}_{tr}}$) preserves the continuity of the function. Finally, $\bar{\imath}_f$ represents the static friction contribution, experimentally identified by providing open-loop increasing steps of current (increments of 5×10^{-3} A), and detecting the start of a continuous motion of the joint.

The feedforward term i_{ff} improves torque tracking performance, accounting for the motor constant k_t, the reduction ratio k_r, and the efficiency η:

$$i_{ff} = (k_t k_r \eta)^{-1} \tau_d \qquad (4)$$

It reduces residual error in case of resistive disturbances potentially exerted by a subject due to the absence of an integral term.

Finally, the presence of a PD controller guarantees loop stability in tracking the desired interaction torque signal.

III. Experiments and Results

A. Bandwidth and torque tracking

The output joint of the actuation unit was mechanically blocked and a preload torque offset was commanded; a torque chirp signal was fed as τ_d, with an amplitude of 0.15 Nm covering a frequency range of [0.01 - 3] Hz in 60 s (Figure 5a). Three trials were performed and the averaged transfer function between τ_d and τ was calculated. In Figure 5b, at 0.1 Hz, the error is 1.6±2.7% with a phase lag of 4.4±0.4°. Overall, the Bode plot does not reach -3dB amplitude and the root-mean-square error between τ_d and τ is lower than 0.06 Nm.

B. Transparency

With the robot in transparent mode, a healthy subject was asked to move the index finger with a frequency that increased linearly over a range suitable for the individual, spanning from 0.01 to 3 Hz. The movements covered a RoM of 40° and were guided by a visual reference displayed on a screen. Six trials were performed, in two conditions, namely with and without friction compensation. The transfer function between the measured torque, normalized by the spring stiffness, and the output joint position was calculated to assess the *residual stiffness* (Figure 5d). It resulted equal to -35.3±0.3 and -38.8±1.7 dB at 1 Hz without and with friction compensation, corresponding to a residual stiffness of 0.18 and 0.12 Nm/rad; this would denote a reduction of the nominal stiffness of the spring by a factor of 58 and 87 respectively. The friction compensation proves to be effective, improving the performance by 32% at 1 Hz.

To quantify the effect of friction compensation at the different movement velocities, time domain data were segmented into single-movement cycles by finding the maxima of the joint angle measure. For each movement cycle, the maximum and mean value of the absolute torque and the maximum value of the absolute velocity were extracted; parameters were averaged across cycles and trials and divided into three frequency ranges for comparison (Figure 7). Comparing the conditions with and without friction compensation in the low ([0-1] Hz) and medium ([1-2] Hz) frequency ranges, the maximum velocity variation was lower than 3% between the two, and a reduction of 32% and 12%

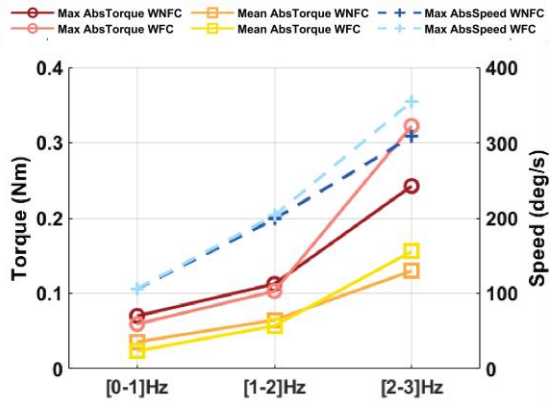

Figure 7 - Time domain transparency indexes in the transparency test. WNFC=with no friction compensation, WFC=with friction compensation

was observed for the mean absolute torque. A smaller variation was observed for the maximum absolute torque, which was reduced by 14% and 9% in the same ranges respectively.

C. *Impedance controller*

Three healthy subjects wearing the exoskeleton were asked to remain passive, and the device performed mobilizations of the finger by commanding to the middle-level controller minimum jerk trajectories of fixed duration (3 s), starting from 0° and with three different target positions (20°, 40°, and 60°), back and forth. For each target position, 10 repetitions were executed, and the protocol was repeated twice, setting a "low" and "high" stiffness parameter (K_p equal to 0.01 $\frac{Nm}{deg}$ and 0.02 $\frac{Nm}{deg}$ respectively).

The mean steady-state error was calculated to assess the performance of the controller. To verify that the users were not actively involved in the movement, EMG activity of the extensor digitorum (ED) was recorded via pre-gelled bipolar Ag/AgCl surface electrodes using the BTS FREEEMG 1000 (BTS Bioengineering, Milan, Italy) system and normalized by the maximum voluntary contraction (MVC) value, acquired prior to the experimental trials as in [17]. The mean error at steady state over the ten repetitions is shown in Figure 6, along with the maximum peak of muscle activity over the cycles for each control condition. The test reports an error positively correlated with the target position, with lower errors for higher stiffness parameters. The third subject presented a maximum error equal to 10° for the low stiffness modality, while the second subject presented a maximum error equal to 5.8° for the high stiffness modality; the standard deviations were always below 1.3° and 0.3°, in the two modalities. The activation of the ED muscle was always lower than 4% of the MVC.

IV. Discussion

The MITEx features an actuation unit with a highly reduced motor group to increase the power-to-dimension ratio, and a torque-sensing element in series to enhance mechanical compliance and enable torque control. Such a

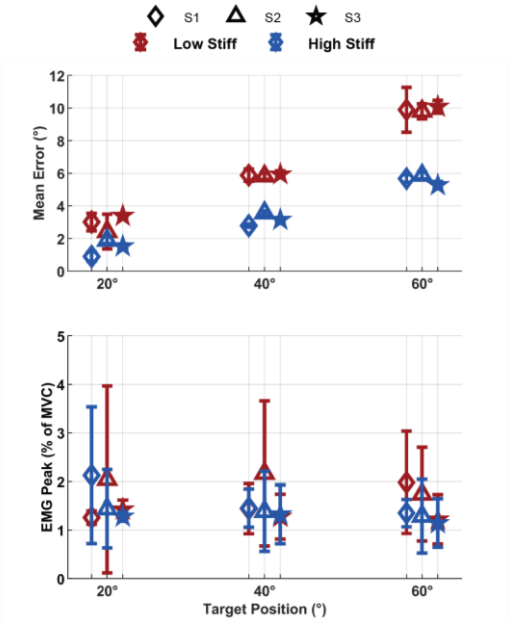

Figure 6 - Mean position error at steady state during *robot-in-charge* modality with stiff (blue) and compliant (red) behavior and EMG subjects activity during the test (right). Diamond, triangle and star account for the three subjects.

solution allows achieving peak torques up to 1.3 Nm, to account also for I-MCP joint hyper-resistance e.g. due to spasticity. Another rigid exoskeleton for index finger with SEA-based cable actuation is capable of providing peak torques of 0.3 Nm, , but assistance is delivered at both MCP and PIP joints with a lower weight on the hand (~110gr) [6]; the device presented in [18] adopts a similar approach in assisting a single DoF, and it can render higher torques (> 5Nm), even if portability of the device was not considered for the specific application.

The actuation unit is placed on the dorsum of the hand to achieve portability and allow users to explore the entire workspace. A similar solution is adopted in [8], but without force feedback for delivering the assistance. The prototype in [9] has an additional actuation unit for the thumb, which in our case is avoided to limit the weight of the device. Nevertheless, the thumb can be locked in specific configurations for pinching and grasping tasks. In addition, lateral positioning of the kinematic chain with respect to the finger was adopted to reduce encumbrances and avoid remote CoR and self-aligning mechanisms. The MITEx has a weight of 470 gr, including also the actuation unit and the p-HRIs, distributed on the user's hand and wrist; two similar devices in the state of the art that also allow exploring the arm workspace for functional tasks have a weight of ~110 gr [6] and 950 gr [9]. Compact electronics eases the deployment of the device in clinical settings while offering the chance to address full portability in a future version; ECAT communication avoids the use of multiple, long wires that may suffer from sensitivity to external disturbances and might undermine the robustness of the hardware with respect to unexpected strain forces. A control strategy is implemented

to render high compliance and high stiffness respectively, for realizing both *patient-in-charge* and *robot-in-charge* control modalities [7].

Torque tracking performance showed a bandwidth higher than 2.5 Hz, suitable for the intended application and comparable with the SEA-based device presented in [6], which showed also lower RMSE even though transparency was not assessed systematically. The transparency test verified the compliance offered by the combination of mechanical and control solutions adopted, with residual torques lower than 10% of the maximum torque. For the transparency evaluation, similar metrics to [19] and [20] were used, without a force sensor, relying on the FSEA configuration adopted. The limitations of the torque control performance can be mainly attributed to the limited encoder resolution, which could be improved by utilizing a custom-made encoder rather than relying on commercially available solutions.

The friction compensation was beneficial up to 2 Hz, which are frequencies mainly involved in a rehabilitation scenario, where slow mobilizations are expected; from 2 Hz on, transparency performance was negatively influenced by the friction compensation, which increased acceleration and consequently the residual torque due to the reflected inertia of the motor. Nevertheless, residual torques remained lower than 0.35 Nm also at higher velocities. Dynamic friction was not characterized since movements with high velocities, which would have non-negligible dynamic friction contribution, are not expected in the scenario considered; moreover, only a partial compensation is required to preserve stability and to prevent the joint from moving in case any volitional torque is not applied at the output stage.

The tests for the impedance controller showed that the device resulted suitable to render different stiffnesses. The intra- and inter-subject standard deviation was always below 1.5°, and the trials in high-stiffness condition showed the highest repeatability. The steady-state error was lower in [18], although, in that case, the characterization did not involve human subjects and was performed within a lower RoM. The increasing trend of the steady-state error in the low-stiffness condition could be due to the compression of soft tissues and interfaces and to the intrinsic stiffness of the anatomical joint, even if the poor sample size does not allow us to draw generalized conclusions.

In conclusion, the presented hand exoskeleton provides users with the possibility to explore the workspace for upper-limb functional tasks or engage in single-joint exercises for the finger by conveniently resting their arm on a dedicated support. In the next future, we intend to test the device with a clinical population to complement the clinical evaluations with precise and quantitative measures of biomechanical parameters.

REFERENCES

[1] P. Tran, S. Jeong, K. R. Herrin, and J. P. Desai, "Review: Hand Exoskeleton Systems, Clinical Rehabilitation Practices, and Future Prospects," *IEEE Trans. Med. Robot. Bionics*, vol. 3, no. 3, pp. 606–622, Aug. 2021, doi: 10.1109/TMRB.2021.3100625.

[2] C. G. Rose *et al.*, "Hybrid Rigid-Soft Hand Exoskeleton to Assist Functional Dexterity," *IEEE Robot. Autom. Lett.*, vol. 4, no. 1, pp. 73–80, Jan. 2019, doi: 10.1109/LRA.2018.2878931.

[3] M. Sarac, M. Solazzi, and A. Frisoli, "Design Requirements of Generic Hand Exoskeletons and Survey of Hand Exoskeletons for Rehabilitation, Assistive, or Haptic Use," *IEEE Trans. Haptics*, vol. 12, no. 4, pp. 400–413, Dec. 2019,doi:10.1109/TOH.2019.2924881.

[4] M. Santello, M. Flanders, and J. F. Soechting, "Postural Hand Synergies for Tool Use," *J. Neurosci.*, vol. 18, no. 23, pp. 10105–10115, Dec. 1998, doi: 10.1523/JNEUROSCI.18-23-10105.1998.

[5] M. Zbytniewska *et al.*, "Reliable and valid robot-assisted assessments of hand proprioceptive, motor and sensorimotor impairments after stroke," *J. NeuroEngineering Rehabil.*, vol. 18, no. 1, p. 115, Jul. 2021, doi: 10.1186/s12984-021-00904-5.

[6] P. Agarwal, *et al.*, "An index finger exoskeleton with series elastic actuation for rehabilitation: Design, control and performance characterization," 2015. https://journals.sagepub.com/doi/10.1177/0278364915598388.

[7] S. Dalla Gasperina, L. Roveda, A. Pedrocchi, F. Braghin, and M. Gandolla, "Review on Patient-Cooperative Control Strategies for Upper-Limb Rehabilitation Exoskeletons," *Front. Robot. AI*, vol. 8, p. 745018, Dec. 2021, doi: 10.3389/frobt.2021.745018.

[8] D. Wang, Q. Meng, Q. Meng, X. Li, and H. Yu, "Design and Development of a Portable Exoskeleton for Hand Rehabilitation," *IEEE Trans. Neural Syst. Rehabil. Eng.*, vol. 26, no. 12, pp. 2376–2386, Dec. 2018, doi: 10.1109/TNSRE.2018.2878778.

[9] D. Leonardis *et al.*, "An EMG-Controlled Robotic Hand Exoskeleton for Bilateral Rehabilitation," *IEEE Trans. Haptics*, vol. 8, no. 2, pp. 140–151, Jun. 2015, doi: 10.1109/TOH.2015.2417570.

[10] C. Lee, *et al.*, "Generalization of Series Elastic Actuator Configurations and Dynamic Behavior Comparison," *Actuators*, vol. 6, no. 3, Art. no. 3, Sep. 2017, doi: 10.3390/act6030026.

[11] F. Just *et al.*, "Exoskeleton transparency: feed-forward compensation vs. disturbance observer," - *Autom.*, vol. 66, no. 12, pp. 1014–1026, Dec. 2018, doi: 10.1515/auto-2018-0069.

[12] E. Peperoni *et al.*, "Self-Aligning Finger Exoskeleton for the Mobilization of the Metacarpophalangeal Joint," *IEEE Trans. Neural Syst. Rehabil. Eng.*, pp. 1–1, 2023, doi: 10.1109/TNSRE.2023.3236070.

[13] M. Cempini, M. Cortese, and N. Vitiello, "A Powered Finger–Thumb Wearable Hand Exoskeleton With Self-Aligning Joint Axes," *IEEEASME Trans. Mechatron.*, vol. 20, no. 2, pp. 705–716, Apr. 2015, doi: 10.1109/TMECH.2014.2315528.

[14] A. Baldoni *et al.*, "Kinematical chain for assisting the motion of a spherical joint," WO2019012429A1, Jan. 17, 2019 Accessed: Dec. 06, 2022. [Online]. Available: https://patents.google.com/patent/WO2019012429A1/en

[15] A. Baldoni, *et al.*, "A planar torsional spring," WO2020104962A1, May 28, 2020 Accessed: Dec. 06, 2022. [Online]. Available:https://patents.google.com/patent/WO2020104962A1/en

[16] M. Hutter *et al.*, "ANYmal - a highly mobile and dynamic quadrupedal robot," in *2016 IEEE/RSJ International Conference on Intelligent Robots and Systems (IROS)*, Oct. 2016, pp. 38–44. doi: 10.1109/IROS.2016.7758092.

[17] E. Capotorti *et al.*, "A Novel Torque-Controlled Hand Exoskeleton to Decode Hand Movements Combining Semg and Fingers Kinematics: A Feasibility Study," *IEEE Robot. Autom. Lett.*, vol. 7, no. 1, pp. 239–246, Jan. 2022, doi: 10.1109/LRA.2021.3111412.

[18] M. Zbytniewska *et al.*, "Design and Characterization of a Robotic Device for the Assessment of Hand Proprioceptive, Motor, and Sensorimotor Impairments," in *2019 IEEE 16th International Conference on Rehabilitation Robotics (ICORR)*, Jun. 2019, pp. 441–446. doi: 10.1109/ICORR.2019.8779507.

[19] J. Pan *et al.*, "NESM-γ: An Upper-Limb Exoskeleton With Compliant Actuators for Clinical Deployment," *IEEE Robot. Autom. Lett.*, vol. 7, no. 3, pp. 7708–7715, Jul. 2022, doi: 10.1109/LRA.2022.3183926.

[20] Y. Zimmermann, A. Forino, R. Riener, and M. Hutter, "ANYexo: A Versatile and Dynamic Upper-Limb Rehabilitation Robot," *IEEE Robot. Autom. Lett.*, vol. 4, no. 4, pp. 3649–3656, Oct. 2019, doi: 10.1109/LRA.2019.2926958.